URTeC: 1341

Quick Evaluation for Optimal Recovery in Unconventional Reservoirs

Reinaldo J. Michelena*[1,2], Huabing Wang[2], and James R. Gilman[2],
1. SeisPetro Geoconsulting, 2. iReservoir.

Abstract

We present a workflow to estimate recovery in unconventional reservoirs that uses flow simulation models constrained by seismic data, geomechanical parameters, and hydraulic stages properties. The goal of the workflow is the rapid testing of different hydraulic stage scenarios in the presence of natural fractures and other hypotheses that can be compared to select the one that yields optimal recovery. All the parameters of interest are generated directly into a flow simulation grid centered on the horizontal well. Thickness of hydraulic stages equals that of one cell of the simulation grid and therefore, details of individual hydraulic fractures are not explicitly considered allowing modeling of larger reservoir scale effects on recovery. The first step is the estimation of natural fracture orientations using seismic data calibrated with independent fracture information. Then, the flow grid is also populated with geomechanical parameters such as stress field and stress orientations, pore pressure, and friction coefficient. After defining locations and geometry of hydraulic stages along the well path and assuming fluid pressure decay functions away from the hydraulic stages, we use Mohr-Coulomb faulting theory to estimate which natural fractures are more prone to reactivation after hydraulic stimulation. This volume of reactivated natural factures is then upscaled to effective fracture permeability that serves as input to an ultra-fast dual-permeability flow simulator. Finally, once the model is in the flow simulator, we use fluid properties and other dynamic parameters for calibrating with production information, changing the simulation model if needed, and performing long term forecast. We illustrate the application of the workflow in the Eagle Ford formation (South Texas) using a data set that consists of 3D seismic, outcrop descriptions, geomechanics measurements, and production information.

Introduction

Unconventional reservoirs are characterized by extremely low permeabilities that hinder fluid communication between the reservoir and the borehole. These permeabilities are enhanced by the generation of hydraulic fractures after high-pressure fluid is injected into the formations of interest. Even though hydraulic fractures are the main source of permeability enhancement near the wellbore, reactivation of existing natural fractures in the vicinity of the hydraulic fractures is also an important mechanism of self-propped permeability enhancement in the stimulated reservoir volume (SRV)

(Gutierrez et al., 2000; Zhang and Li, 2016; Rutledge and Phillips, 2003) and the hydraulic fractures regions (Jeffrey, 2010; Maxwell, 2011).

Reactivation of existing natural fractures depends on the current state of stress, orientation and intensity of existing natural fractures relative to the stress field, injected fluid pressures, rock properties, and geometry of hydraulic stages. In this paper, we consider all these parameters in an integrated fashion that uses Mohr-Coulomb faulting theory to estimate the likelihood of slip of existing natural fractures. Then, we use simple aperture versus fluid pressure assumptions to generate effective permeability volumes of reactivated fractures.

Previous studies about natural fracture reactivation for a given stress field (Bayer et al., 2016; Dershowitz et al., 2019; Evans et al., 2019) rely on the generation Discrete Fracture Models (DFMs) that are used as input for the geomechanical computations and permeability upscaling. This approach has two important limitations. First, although DFMs are useful for visual representation of natural fracture models and can incorporate detailed information about the fractures themselves, their generation and calibration are both cumbersome and time-consuming. The laborious nature of DFM modeling makes the generation of different scenarios more difficult and therefore, typically only one case is considered. The second limitation is that, since flow simulation models require a continuum representation of input permeability models (in "sugar cube" type of grids), DFMs results must be upscaled to the continuum before they can be used for flow simulation, resulting in an extra effort that adds both complexity and time.

In this paper, we build Continuous Fracture Models (CFMs) to represent natural fractures properties. These models are constrained by seismic derived natural fracture orientations that helps introduce real lateral and vertical heterogeneities into the permeability modeling workflow. By using CFMs, different scenarios of natural fracture orientations can be easily generated and the computations related to fracture reactivation and permeability upscaling are significantly faster compared to DFM approaches.

Due to computational constraints, commercially available applications for hydraulic fracture modeling (e.g., Barree, 1983, and McClure at al., 2016) typically select only a portion of the well to model the details and complexities of the propagation of individual hydraulic fractures. Modeling the entire well to include the expected geologic variations is beyond the scope of the typical modeling effort due to high computational cost. Our approach, on the contrary, uses effective permeability enhancements at stage scale to be able to analyze the effect of the stimulation in the reservoir volume around the entire well path.

High resolution permeability models generated from this workflow are imported into a GPU-based, dual media flow simulation (Mukundakrishnan et al., 2015) for rapid testing of sensitivities to different parameters and selection of a hydraulic stages design that yields an optimal field recovery.

We start by reviewing the basic theory of natural fracture reactivation from hydraulic stimulation and list the required input data and main assumptions. Then, by using a data set from the Eagle Ford formation in South Texas, we illustrate the application of the workflow to the estimation of production rates from different hydraulic stage scenarios. The input data consists of 3D seismic, geomechanical, and production information. The application starts by the mapping of natural fractures orientations in the reservoir volume using seismic data. Then, we analyze which orientations are more prone to reactivation and transform these volumes of reactivated fractures into volumes of effective fracture permeability. Finally, after building permeability models that correspond to different hydraulic stage scenarios, we perform flow simulation on the different scenarios and compare their corresponding production rate forecasts.

Theory and/or Methods

Review of natural fracture reactivation

Figure 1 shows the relative scales of hydraulic fractures and natural fractures that can be expected in an unconventional reservoir. This figure is a modification of an outcrop map of the Eagle Ford formation by Ferrill et al. (2014) that originally covers an area of about a fourth of a seismic bin size. Two types of

natural fractures are visible in the outcrop: joints (or bed-bound fractures) and small faults (sometimes referred to as through-going fractures). The first observation from this figure is the ubiquitous presence of natural fractures near a typical hydraulic fracture. Ferrill et al. report that small faults are about 4 ft in height and joints are confined to beds of 1 ft or less. Both types of fractures have different flow properties. Whereas faults are sparser and tend to show higher vertical permeability connecting beds of different properties, joints don't contribute much to the vertical connectivity but their abundant character may help enhance lateral fluid flow.

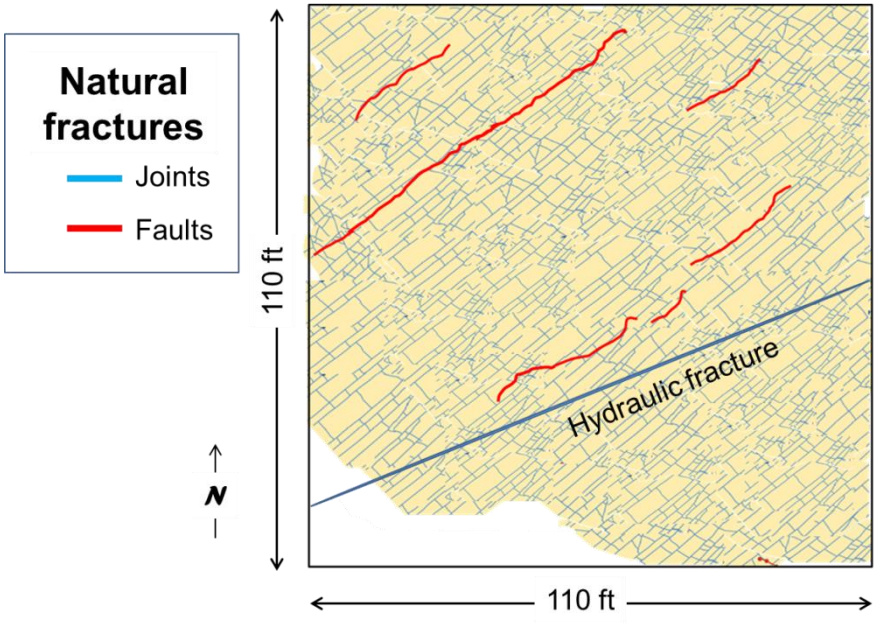

Figure 1. Conceptual scales of fractures relative to a typical seismic bin. This figure is a modification of an outcrop map of the Eagle Ford formation by Ferrill et al. (2014) that originally covers an area of about a fourth of a bin size. Size of faults (in red) has been modified from Ferrill et al.'s original map to include the possibility of small faults crossing the whole cell. AAPG ©2014, reprinted by permission of the AAPG whose permission is required for further use.

For a given background stress field and fractures orientations, we can estimate the likelihood to slip of existing natural fractures using Mohr-Coulomb faulting theory (Zoback and Kohli, 2019). As the fluid pressure is increased from its initial background state, the effective normal stress σ_n acting upon a fracture plane decreases producing shear slip (reactivation) when the extra pressure ΔP is such that the friction coefficient is exceeded. This ΔP is given by the expression

$$\Delta P = (\mu\sigma_n - \tau)/\mu\,, \quad (1)$$

where μ is the coefficient of friction and τ is the shear stress. Positive values of ΔP indicate that the fracture plane of interest hasn't been reactivated whereas negative values indicate that reactivation has occurred.

The mechanism of natural fracture reactivation starts by high-pressure fluid (used to create the hydraulic fractures) leaking off into the abundant natural fractures in their vicinity. Fluid pressure inside the natural fractures is increased, reactivating those that are favorably oriented. Figure 2, modified from Zoback and Lund Snee (2018), illustrates this concept using Formation Micro Imager (FMI) data from a horizontal well in the Barnett Shale. As the fluid pressure is increased, other less favorable orientations are also reactivated creating a "network" of conductive fractures. Both joints and more conductive small faults (Figure 1) may get reactivated. The process continues until the fluid pressure reaches the hydro-fracture limit (~ Shmin). For well planning and design purposes, it is not only important to know which fractures will get reactivated during hydraulic stimulation, but also which fractures will not be reactivated. Fluid pressures much greater that the physical hydro-fracture limit would be required to reactivate unfavorably

oriented natural fractures. Natural fractures that are not reactivated will not contribute to the drainage of the reservoir.

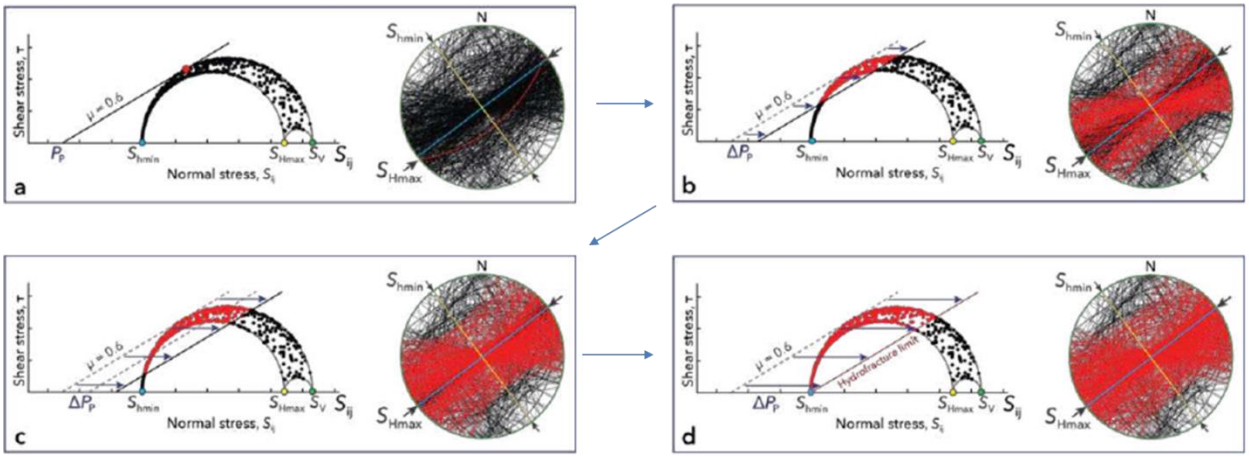

Figure 2. Mohr and stereonet plots indicating the natural fractures interpreted from FMI data. Those that are expected to reactivate as pore pressure increases during hydraulic stimulation are colored red. As pore pressure increases (i.e., friction line moves to the right), more fractures get reactivated (figures a to c) until the maximum injection pressure is reached (d). Many fractures remain closed after this limit is reached. (Modified from Zoback and Lund Snee, 2018).

Input data and assumptions

In this paper, we generalize to 3D the idea presented by Zoback and Lund Snee (2018) in 1D along a horizontal well (Figure 2). Unlike their approach that uses fracture orientations derived from image logs, we use spatially varying fracture orientations derived from 3D seismic data and the following input data and/or assumptions:

1) Stress magnitudes (Sv, Shmax, and Shmin) and orientations.
2) Initial pore pressure.
3) Coefficient of friction.
4) Hydraulic stage geometry, effective permeability, and fluid pressure.
5) Pressure decay function away from hydraulic fractures.

All these parameters are generated in a common flow simulation grid of 50ft *x* 50ft *x* 10ft cell size. Then, we solve equation 1 for each cell of the grid to decide which orientations are more prone to reactivation.

Results

Continuous model of natural fractures from seismic data

Local orientations were derived from maximum curvature extracted from seismic data. After careful calibration with orientations of joints and faults from outcrop data, we concluded that orientations derived from maximum curvature could be used as a proxy for orientations of actual natural fractures in the area. For more details, see Michelena et al. (2019).

Figure 3a shows the well path of interest in the depth domain. The horizontal section of this well is approximately 7300 ft. Figure 3b shows the seismic maximum curvature in the volume around the horizontal well. Figure 3c shows the average orientations derived from the maximum curvature. Figure 3d shows a histogram of these orientations. Three main families of orientations are observed along the vicinity of the well. The dominant family of orientations at approximately N45E is roughly 25 degrees

away from the orientation of maximum horizontal stress. This family of orientations is the first one that will reactivate under hydraulic stimulation.

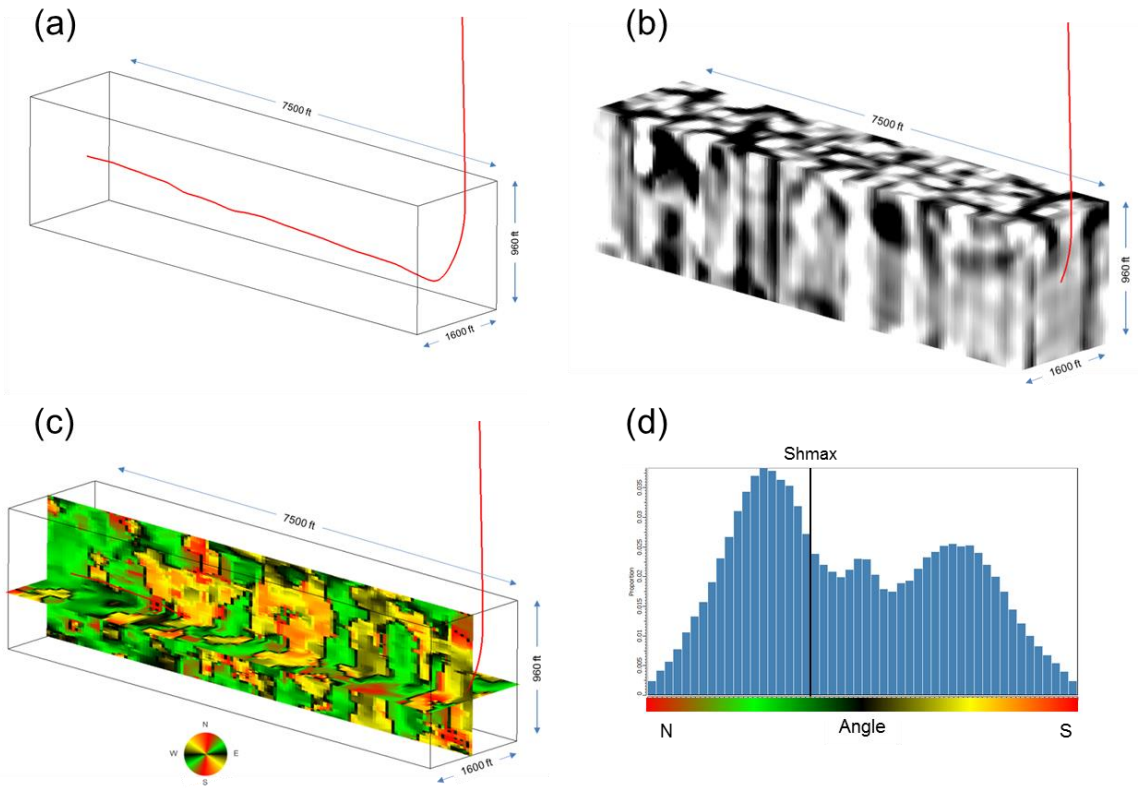

Figure 3. (a) Well path and volume of interest around it. The dimensions of the volume of interest are 7500 ft *x* 1600 ft *x* 960 ft. (b) Seismic maximum curvature. (c) Average orientations derived from maximum curvature. (d) Histogram of orientations derived from maximum curvature. Orientation of maximum horizontal stress is also indicated in the histogram.

Model of reactivated fractures: stresses, hydraulic fractures, and fluid pressures

The geomechanical information used to solve equation 1 consisted of vertical stress Sv for the depths of interest, measured Shmin at the same depths, and estimated Shmax. Relative values of stresses in the area indicate a normal faulting regime. No lithofacies constraints were used in this example to differentiate areas more or less prone to fracture reactivation based on clay content. Pore pressure at the depth of interest was also available. These values were transformed into gradients that were used to populate the 3D grid with the different geomechanical parameters.

We modeled 11 stages of hydraulic fracturing. Stages are 600 ft apart (Figure 4a). We also assumed a constant fluid pressure equal to Shmin within the hydraulic fractures and following Mukuhira et al. (2016), we assumed a linear fluid pressure decay away from the hydraulic fracture for the injection phase of the stimulation (Figure 4b). Observations from microseismic data in the area were also used to estimate the distance where excess fluid pressure decayed to zero.

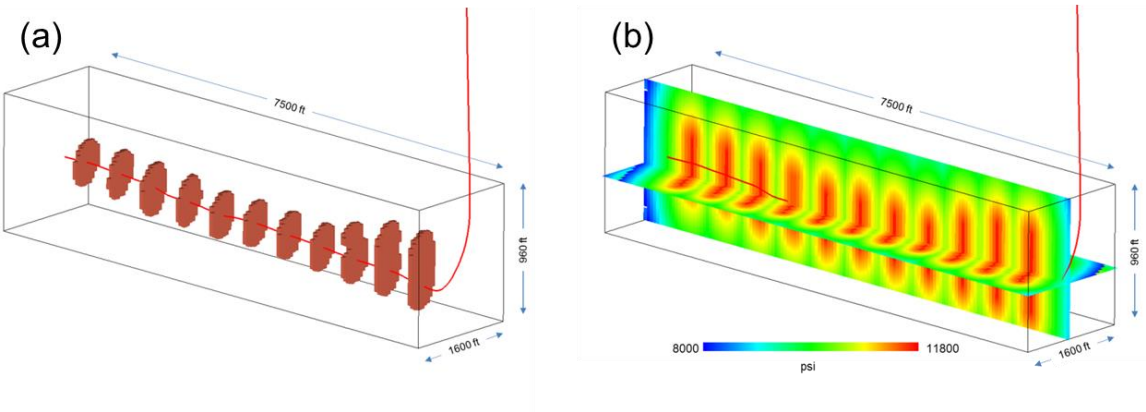

Figure 4. (a) Hydraulic fractures along horizontal well. Half-length of each stage is 400 ft and half-height is 150 ft. (b) Assumed fluid pressure decay away from hydraulic fractures.

Equation 1 was used to determine whether the average fracture orientation in each grid cell was likely to get reactivated after increasing fluid pressure. The result is shown in Figure 5a. Blue points above the friction line indicate natural fractures that have been reactivated (conductive) whereas red points below the friction line indicate fractures that remain closed. Figure 5b shows the distribution of reactivated and closed fractures in 3D space around the well. As expected, more natural fractures get reactivated near the hydraulic fractures than farther away from them. The heterogeneous nature of the SRV around each hydraulic fracture depends on the variability of local fracture orientations and hence the need to simulate the entire well and not only a few stages.

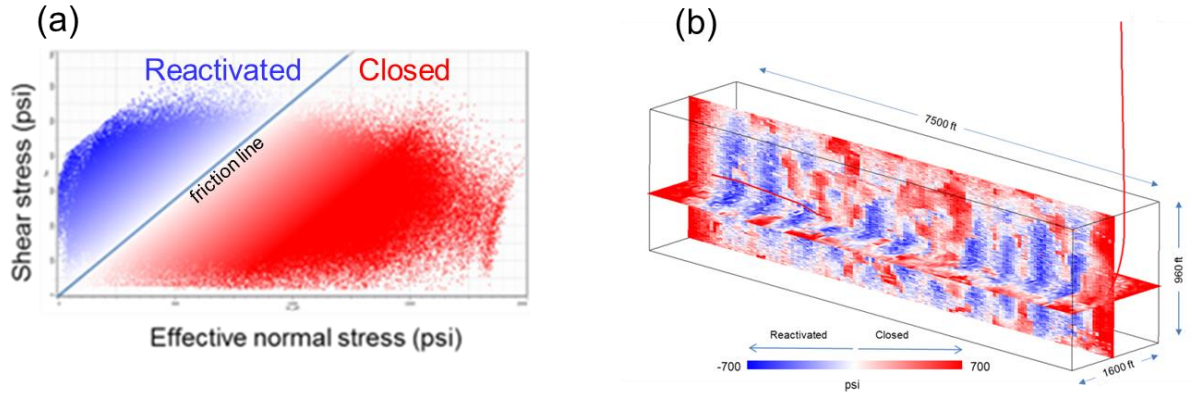

Figure 5. (a) Effective normal stress versus shear stress colored by ΔP calculated from equation 1. Each point represents a natural fracture orientation in the simulation grid. (b) Volume of reactivated and closed natural fractures around the well path.

Effective permeability of reactivated fractures

The model of reactivated natural fractures shown in Figure 5b was upscaled to effective permeability using the Oda equation (Oda, 1985). The effective fracture permeability tensor is proportional to the sum of the product of individual fracture permeabilities, fracture porosity, and a geometric factor related to the fracture orientations, as follows:

$$k_{eij} \propto \sum_{k=1}^{N_f} \left(\frac{w_f^2}{12}\right)_k \left(\frac{w_f A_f}{\Delta x \Delta y \Delta z}\right)_k \left(n_i n_j\right)_k, \qquad (2)$$

where k_{eij} is the effective fracture permeability for the total number of fractures N_f, w_f is the fracture aperture, A_f is the fracture area, $\Delta x \Delta y \Delta z$ is the cell volume, and n_i is the projection of the normal to the fracture k along the i^{th} axis. The effect of scale on effective permeability is not only related to the cell volume but also to the number of cells involved in the summation. After defining fracture areas and

apertures, we apply equation (2) in a moving average fashion on the 3D grid to obtain a permeability tensor per cell. Measured permeabilities or existing production data are required to calibrate the apertures. Natural fractures reactivated at higher pressure (or low effective normal stress) will have higher permeability than those reactivated at lower pressure (Zhang and Li, 2016; Rutter and Mecklenburgh, 2018). For this reason, our model for the relation between fracture aperture and fluid pressure results in fractures reactivated far from the hydraulic stages having a significantly lower contribution to flow than fractures reactivated near the hydraulic stages. The aperture model can also include expected effects of proppant in hydraulic fracture and natural fracture conductivity (Montgomery et al., 2020).

The outputs of the Oda upscaling are k_{max} (maximum permeability), k_{min} (minimum permeability) and orientation of k_{max}. The effective fracture permeability k_T in each cell of the simulation grid is calculated as

$$k_T = k_{HF} + k_e \,, \qquad (3)$$

where k_{HF} is the effective, enhanced permeability within the hydraulic stage (zero outside), and k_e is the effective permeability of reactivated natural fractures calculated as $\sqrt{k_{max}k_{min}}$. The effective fracture permeability is assigned to the fracture network in the dual-permeability model. The matrix permeability, k_m , is modeled separately and represents the matrix contribution of the dual-permeability grid.

Figure 6a shows the heterogeneity in the effective permeability of reactivated fractures k_e along the hydraulic stages. Some portions of the stages are more permeable than others. This heterogeneity is due to the variability of natural fracture orientations within the stages, as shown in Figure 6b. Natural fractures whose orientations are perpendicular to Shmax are not reactivated and therefore, do not benefit from permeability enhancement. To estimate k_{HF} (equation 3) in this particular example, we used a multiplier to the reactivated fractures k_e within the stages.

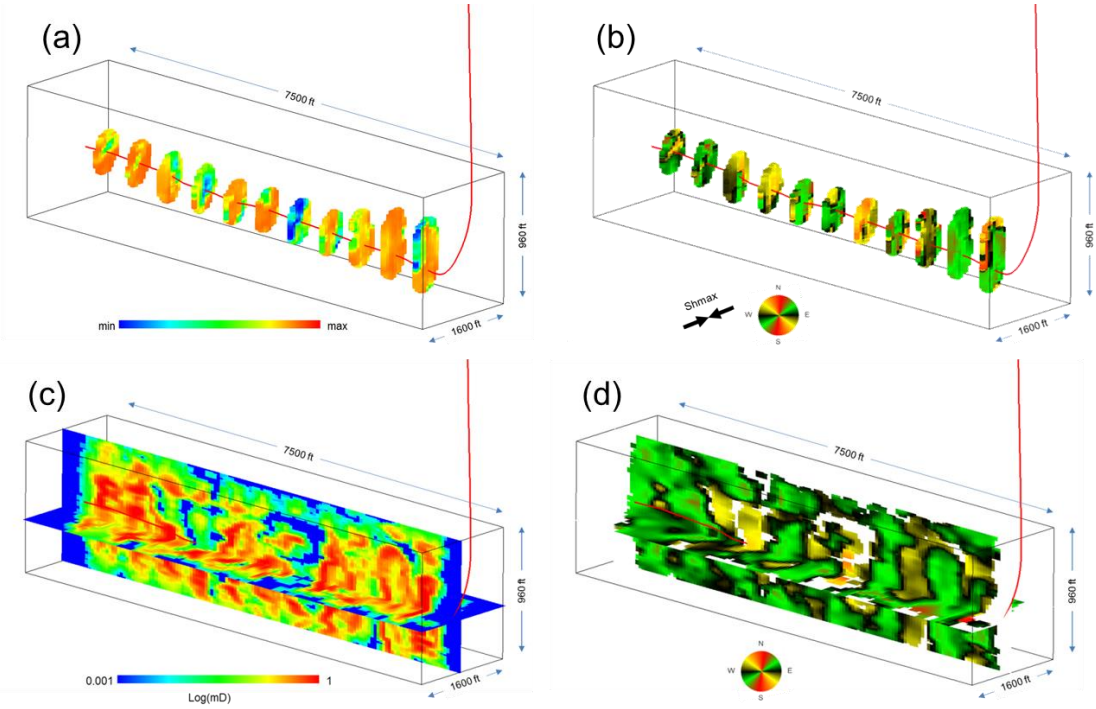

Figure 6. (a) Effective permeability k_e of reactivated fractures within hydraulic stages. (b) Orientations of natural fractures within hydraulic stages. Permeabilities of poorly oriented natural fractures within hydraulic stages are not enhanced. (c) Volume of k_e around the well path. Permeability of hydraulic stages is not considered in this figure. (d) Orientation of maximum effective permeability of reactivated fractures.

Figure 6c shows the effective permeability k_e from Oda upscaling applied to the reactivated fractures shown in Figure 5b. The effective permeability enhancement is significantly heterogeneous due to

geologic variability and decaying fluid pressures. Some areas (in blue) are not reactivated and remain at their initial matrix permeability. Other areas show a permeability enhancement of about 3 orders of magnitude, from 0.001 md (matrix permeability) to 1 md. Figure 6d shows the orientation of maximum permeability in the reactivated areas. As expected from Figure 2, these orientations are close to the orientation of Shmax. Orientations nearly perpendicular to Shmax remain non-conductive.

Flow simulation

Matrix porosity and permeability, fracture porosity, fracture permeability, shape factor (related to fracture intensity), and fluid properties are the parameters that control fluid flow in naturally fractured reservoirs. Whereas the distribution of matrix porosity and permeability is constrained by log and seismic data using prestack inversion results and facies mapping, the distribution of permeability of reactivated fractures is based on the results of the Oda upscaling as previously explained. The purpose of flow simulation is to understand how these parameters interact with one another for different stimulation scenarios or assumptions (e.g., hydraulic stage geometries, fluid pressures or aperture enhancements) resulting in different initial production rates, decline, and ultimate recoveries. Early production data (rates and pressures) is used to calibrate the models. Our workflow uses an efficient dual permeability, GPU-based flow simulator (Mukundakrishnan et al., 2015) that allows a very fine grid description of the fracture heterogeneity, matrix property variations, and long-term pressure mapping while still allowing rapid evaluation of the impact of different geologic and hydraulic stage scenarios on the ultimate recovery of hydrocarbons.

To illustrate the use of our workflow to forecast oil rates for the well and natural fracture orientations shown in Figure 3, we built permeability models of reactivated natural fractures for different scenarios of geometries and spacing of hydraulic stages along the well path. We considered three scenarios of hydraulic stages along the well path: 11 stages (Figure 4a), 16 stages, and 21 stages. To test the effect of the stage geometry on the recovery, dimensions of individual stages for the cases of 16 and 21 were assumed to be about one-half of the dimensions of the longer spaced stages (11). Apertures of reactivated natural fractures were calibrated with production data from the field. Fluid pressures away from the well were also calibrated with production and microseismic data in the area. Figure 7 shows the result of the flow simulation for the different scenarios. Although initial rates are different for two scenarios, all of them result in a similar long-term forecast, which means that, for this particular case, the selection of the optimal scenario should be based on the economics and not on the expected recovery.

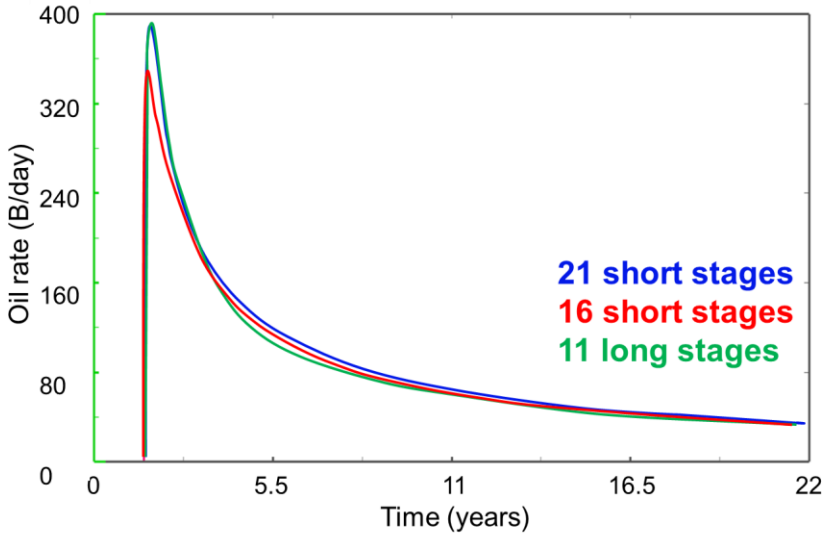

Figure 7. Predicted oil rates from flow simulation along the horizontal well shown in Figure 3a for different geometries and spacing of hydraulic stages. In this particular case, for the natural fracture variability observed around this well (Figure 3c), different scenarios of geometries and spacings result in similar rates.

Discussion

Our goal is the estimation of long-term recovery in unconventional reservoirs from different stimulation scenarios using flow simulation. The resolution of the flow simulation grid defines the fundamental scale to model different phenomena and parameters. The total permeability required for the flow simulator results from defining three permeability contributions for each cell: matrix, hydraulic fractures, and reactivated natural fractures. We use a dual-permeability grid to separately model the matrix and fracture contributions. Long term production is controlled by the effective permeabilities of reactivated fracture and hydraulic stages.

The main contribution of this paper is a workflow to estimate the natural fracture permeability term in equation 3 (Figure 8). The first step is the mapping of 3D seismic data unto a simulation grid, generation of 3D structural attributes, and extraction of local fracture orientations. Then, in the same grid, we define the locations and geometries of the hydraulic stages along the well path and populate the grid with geomechanical parameters. After assuming a fluid pressure decay function in the reservoir, we model which natural fracture orientations are more likely to get reactivated under the assumed pressure conditions. Then, we upscale the natural fracture permeabilities of conductive fractures to effective fracture permeabilities using a moving-average-like approach based on the Oda equation. The results of the permeability upscaling are volumes of permeabilities and orientations of maximum and minimum flow that are then imported into the flow simulator.

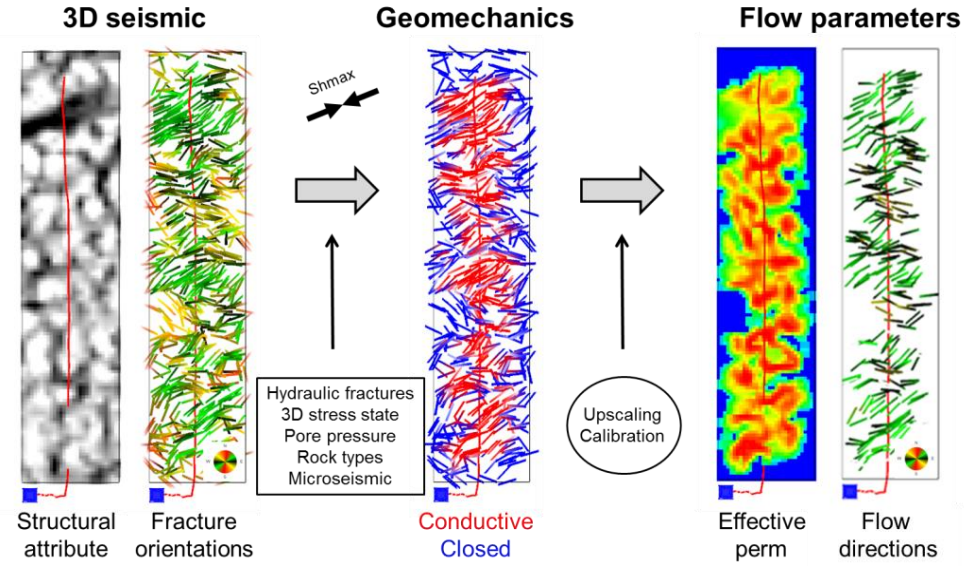

Figure 8. Summary of the seismic-geomechanics-permeability modeling workflow.

To account for the permeability of hydraulic fractures in equation 3, we model equivalent "flow simulation scale" hydraulic stages whose thickness equals the thickness of one cell in the simulation grid (~ 25-50 ft). Although this scale does not allow modeling all the complexities of individual hydraulic fractures and detailed effects of different completion parameters, it does allow capturing the effective permeability enhancements that influence long term recovery at the reservoir scale. By increasing the scale at which we model the perm enhancement due to hydraulic stimulation, we are able to bring into the analysis reservoir scale heterogeneities and effective natural fracture perms *away* from the hydraulic stages that are often ignored but impact long term recovery.

Permeabilities and lateral extent of hydraulic stages can be set in different ways. A simple way is to use a constant matrix permeability multiplier within individual stages. Another way is to use conceptual models derived from hydraulic fracture modeling applications to guide the perm enhancement at selected cells. In

the examples presented in this paper, we use a multiplier to the effective permeabilities of reactivated fractures to model the perms inside hydraulic stages whose geometry is set by conceptual considerations.

Another important aspect of our workflow is the use of 3D seismic data to constrain the spatial variability of a continuous natural fracture model of the reservoir. By introducing geologic heterogeneities from seismic data, we are able to evaluate the effectiveness of the recovery around individual stages along the well path. The modeling of natural fractures in the continuous domain also offers several advantages. From the computational point of view, it helps speed up both the estimation of fractures prone to reactivation and the permeability upscaling. Also, from the modeling point of view, it simplifies the generation of different scenarios related to natural fracture distribution.

The other aspect of the workflow that accelerates the generation of production forecasts for the different scenarios is the use of a fast, GPU-based dual permeability flow simulator. Simulation runs typically require just a few minutes allowing many sensitivity iterations in a detailed grid. By using a fine grid, we are not only able to model early time pressure responses but also long-term pressure changes over large distances.

Since all rock properties are mapped unto a simulation grid, the workflow can take into account not only variability in natural fracture orientations from seismic data but also any other rock properties or geomechanical parameters. For example, lateral and vertical frac barriers from seismic derived facies volume can be used to constrain the fracture reactivation, as well as spatially varying Sv, Shmin, or pore pressure derived from log or seismic data.

Conclusions

This paper presents a workflow to perform rapid testing of different recovery scenarios in unconventional reservoirs. At the core of the workflow is a methodology to estimate effective fracture permeability of reactivated, seismic derived natural fracture orientations in the reservoir zone after hydraulic fracture stimulation. First, natural fracture orientations are estimated using seismic data calibrated with independent fracture information. Then, the flow grid is populated with geomechanical parameters such as stress field and stress orientations, pore pressure, and friction coefficient. The thickness of hydraulic stages corresponds to one cell of the flow simulation grid and their overall geometry and effective properties can be based on concepts from hydraulic fracture simulation software or prior experience. After defining geometry and location of hydraulic stages along the well path and assuming fluid pressure decay functions away from the hydraulic stages, we use Mohr-Coulomb faulting theory to estimate which natural fractures are more prone to reactivation in the stimulated volume. This volume of reactivated natural factures is finally upscaled to effective fracture permeability using the Oda equation and the results are imported into a fast, GPU-based dual permeability flow simulator.

The scale of the modeling is defined by the size of the cells in the flow simulation grid. This allows us to focus on reservoir scale variables that impact long term production for rapid testing of scenarios. The workflow can be generalized to consider heterogeneities of rock properties, pressures, stresses, and other geomechanical parameters that impact recovery in the reservoir interval.

The combination of continuous fracture models, fundamental geomechanics concepts, and an ultra-fast flow simulator allow the evaluation of different scenarios of rock properties, fluid properties, stresses, and hydraulic stages for better design of hydraulic stimulation jobs in unconventional reservoirs.

Acknowledgements

Thanks to Hai-Zui Meng and Michael Uland from iReservoir for many important suggestions and enlightening conversations.

References

Barree, R. D., 1983, A Practical Numerical Simulator for Three-Dimensional Fracture Propagation in Heterogeneous Media: SPE Symposium on Reservoir Simulation, 403-414. doi:10.2118/12273-MS.

Bayer, W.S., Wunderle, M., Araujo, E., Alcalde, R., Yao, C., Suhy, F., Jo, T., Bases, F., Sani, A.M., Ma, Y., Bansal, A., Peterson, E., Goudge, R., Awasthi, A., and Bhatia, M., 2016, Geological and Geomechanical Modeling of the Haynesville Shale: a Full Loop for Unconventional Fractured Reservoirs: SEG Global Meeting Abstracts: 2112-2137. https://doi.org/10.15530/urtec-2016-2460295.

Dershowitz, W., Hosseinpour, H., and Cottrell, M., 2019, A Geomechanical Approach for Evaluating Hydraulic Stimulation in Complex Stratigraphies: SEG Global Meeting Abstracts: 5417-5422. doi:10.15530/urtec-2019-945.

Evans, K., Toth, R., Ore, T., Smith, J., Bannikova, N., Carr, T., and Ghahfarokhi, P., 2019, Fracture Analysis Before and After Hydraulic Fracturing in the Marcellus Shale using the Mohr-Coulomb Failure Criteria: SEG Global Meeting Abstracts: 4036-4046. doi:10.15530/urtec-2019-650.

Ferrill, D.A., McGinnis, R.N., Morris, A.P., Smart, K.J., Sickmann, Z.T., Bentz, M., Lehrmann, D., and Evans, M.A., 2014, Control of Mechanical Stratigraphy on Bed-Restricted Jointing and Normal Faulting: Eagle Ford Formation, South-Central Texas, U.S.A.: AAPG Bulletin, **98**, 2477-2506. https://doi.org/10.1306/08191414053.

Gutierrez, M.S., Oino, L.E., and Nygaard, 2000, Stress-Dependent Permeability of a De-Mineralised Fracture in Shale: Marine and Petroleum Geology, **17**, 895-907. https://doi.org/10.1016/S0264-8172(00)00027-1

Jeffrey, R.G., Zhang, X., and Bunger, A.P., 2010, Hydraulic Fracturing of Naturally Fractured Reservoirs: Proceedings of the Thirty-Fifth Workshop on Geothermal Reservoir Engineering, Stanford University, SGP-TR-188.

Maxwell, S.C., 2011, What Does Microseismic Tell us About Hydraulic Fracture Deformation: Recorder, 36, 30-45.

McClure, M. W., Babazadeh, M., Shiozawa, S., and Huang, J., 2016, Fully Coupled Hydromechanical Simulation of Hydraulic Fracturing in 3D Discrete-Fracture Networks: SPE Journal, 21, 1302-1320. doi:10.2118/173354-PA.

Michelena, R.J., Gilman, J.R., and Zahm, C.K., 2019, Seismic, Geologic, Geomechanics, and Dynamic Constraints in Flow Models of Unconventional Fractured Reservoirs: Example From a South Texas Field: The Leading Edge, **38**, 116-122. https://doi.org/10.1190/tle38020116.1.

Montgomery, C.T., Smith. M.B., An, Z., Klein. H.H., Strobel. W., and Myers, R.R., 2020, Utilizing Discrete Fracture Modeling and Microproppant to Predict and Sustain Production Improvements in Nano Darcy Roc, SPE-199741-MS. https://doi.org/10.2118/199741-MS

Mukuhira, Y., Dinske, C., Asanuma, H., Ito, T., and Häring, M. O., 2017, Pore Pressure Behavior at the Shut-in Pphase and Causality of Large Induced Seismicity at Basel, Switzerland: J. Geophys. Res. Solid Earth, 122, 411-435. doi:10.1002/2016JB013338.

Mukundakrishnan, K., Esler, K., Dembeck, D., Natoli, V., Shumway, J., Zhang, Y., Gilman, J., and Meng, H., 2015, Accelerating Tight Reservoir Workflows With GPUs: SPE-173246-MS, Extended Abstracts. https://doi.org/10.2118/173246-MS.

Oda, M., 1985, Permeability Tensor for Discontinuous Rock Masses: Géotechnique, **35**, 483-495. https://doi.org/10.1680/geot.1985.35.4.483

Rutledge, J.T. and Phillips, W.S., 2003, Hydraulic stimulation of natural fractures as revealed by induced microearthquakes, Carthage Cotton Valley gas field, east Texas: Geophysics, **68**, 441-452. https://doi.org/10.1190/1.1567214.

Rutter, E.H., and Mecklenburgh, J., 2018, Influence of normal and shear stress on the hydraulic transmissivity of thin cracks in a tight quartz sandstone, a granite, and a shale: Journal of Geophysical Research: Solid Earth, **123**, 1262–1285. https://doi.org/10.1002/2017JB014858.

Zhang Z., and Li, X., 2016, The Shear Mechanisms of Natural Fractures During the Hydraulic Stimulation of Shale Gas Reservoirs: Materials, **9**, 713-726. doi:10.3390/ma9090713.

Zoback, M.D., and Lund Snee, J.-E, 2018, Predicted and Observed Shear on Pre-Existing Faults During Hydraulic Fracture Stimulation: SEG Expanded Abstracts, 3588-3592. https://doi.org/10.1190/segam2018-2991018.1

Zoback, M.D., and Kohli, A.H., 2019, Unconventional Reservoir Geomechanics: Cambridge University Press.